Contents lists available at ScienceDirect

JOURNAL of ASIAN CERAMIC SOCIETIES

Journal of Asian Ceramic Societies

journal homepage: www.elsevier.com/locate/jascer

Finite element analysis of vibration energy harvesting using lead-free piezoelectric materials: A comparative study

Anuruddh Kumar*, Anshul Sharma, Rajeev Kumar, Rahul Vaish, Vishal S. Chauhan

School of Engineering, Indian Institute of Technology Mandi 175001, Himachal Pradesh, India

ARTICLE INFO

Article history:
Received 10 October 2013
Received in revised form 17 January 2014
Accepted 1 February 2014
Available online 22 February 2014

Keywords:
Lead-free piezoelectric materials
Energy harvesting
Unimorph cantilever configuration
Finite element analysis
Genetic algorithm

ABSTRACT

In this article, the performance of various piezoelectric materials is simulated for the unimorph cantilever-type piezoelectric energy harvester. The finite element method (FEM) is used to model the piezolaminated unimorph cantilever structure. The first-order shear deformation theory (FSDT) and linear piezoelectric theory are implemented in finite element simulations. The genetic algorithm (GA) optimization approach is carried out to optimize the structural parameters of mechanical energy-based energy harvester for maximum power density and power output. The numerical simulation demonstrates the performance of lead-free piezoelectric materials in unimorph cantilever-based energy harvester. The lead-free piezoelectric material $K_{0.5}Na_{0.5}NbO_3$-$LiSbO_3$-$CaTiO_3$ (2 wt.%) has demonstrated maximum mean power and maximum mean power density for piezoelectric energy harvester in the ambient frequency range of 90–110 Hz. Overall, the lead-free piezoelectric materials of $K_{0.5}Na_{0.5}NbO_3$-$LiSbO_3$ (KNN-LS) family have shown better performance than the conventional lead-based piezoelectric material lead zirconate titanate (PZT) in the context of piezoelectric energy harvesting devices.

1. Introduction

Vibration energy harvesting is defined as the conversion of vibration energy into electrical energy. Current solutions for vibration-to-electricity conversion are mostly accomplished via electrostatic [1–3], electromagnetic [4–7], or piezoelectric principles [8–10]. Among the available vibration energy harvesting methodologies, piezoelectric-based approaches are widely recognized because of the relatively high energy density [11]. Piezoelectric materials have been explored significantly for a diversified range of sensor, actuator and energy harvesting applications [11–16]. Various designs of piezoelectric energy harvesters have been proposed [17]. Cantilever beam-based vibration energy harvesters are found to be the simplest and versatile design and hence are studied extensively. Maximum system performance can be achieved when the cantilever is tuned to match its resonance frequency with the external excitation frequency. Material properties that control the performance of piezoelectric energy harvesters are dielectric constant, piezoelectric strain coefficient, electromechanical coupling coefficient, Young modulus, density, and electrical and mechanical quality factors. The above-mentioned favorable properties cannot be associated with one single material. However, lead-based materials have been reported for their best performance among all the known piezoelectric materials [9,18–23]. It is to be noted that lead has a negative impact on environment because of its toxicity. Most of the countries have barred the use of lead in all applications. In this context, scientists are now working toward new materials with comparable or better performance than that of lead-based materials. A number of lead-free piezoelectric ceramics are reported for various promising device applications [24–29]. Our group performed material selection studies for piezoelectric applications using quantitative multiple attribute decision-making approaches. We found that $K_{0.5}Na_{0.5}NbO_3$ (KNN)-based materials are promising piezoelectric materials for futuristic applications [30–32].

A pool of articles has been published on the physical properties of lead-free piezoelectric ceramics. However, their real time performance is not simulated and compared with lead-based materials in energy harvesting applications. The present article demonstrates the numerical simulations for the performance of lead-free piezoelectric materials in unimorph cantilever-type energy harvesters. The performance of lead-free piezoelectric materials is compared with the performance of conventional lead zirconate titanate (PZT) for mechanical vibration-based cantilever piezoelectric harvester.

* Corresponding author. Tel.: +91 9418736393; fax: +91 1905 237945.
E-mail address: anuruddh07@gmail.com (A. Kumar).

Peer review under responsibility of The Ceramic Society of Japan and the Korean Ceramic Society.

ELSEVIER Production and hosting by Elsevier

2187-0764 © 2014 The Ceramic Society of Japan and the Korean Ceramic Society. Production and hosting by Elsevier B.V. All rights reserved.
http://dx.doi.org/10.1016/j.jascer.2014.02.001

Table 1
Piezoelectric materials and their properties.

Piezoelectric materials	Young's modulus (E), GPa	Piezoelectric constant (e_{31}), C/m	Dielectric constant (ε), F/m (10^{-9})	Poisson's ratio (υ)	Density (kg/m^3)
KNN-LS-CT (2 wt.%) [35]	120.48	14.4	9.014	0.39	4550
KNN-LS-CT (1 wt.%) [35]	113.64	16.2	10.319	0.39	4550
KNN-LS [35]	82.64	15.4	13.809	0.39	4550
PZT [34]	62	14.9	16.5	0.28	7800
ZnO [33]	29	0.2	9.6	0.3	5680
BNKLBT [36]	110.5	3.91	3.916	0.278	5780

Finite element method (FEM) based on first-order shear deformation theory is used to simulate the results and Genetic Algorithm (GA) is applied to optimize the thickness of host structure, load resistance and length of proof mass for optimum power density.

2. Materials and methods

2.1. Materials

The piezoelectric materials under study consist of lead-based piezoelectric materials as well as lead-free piezoelectric materials that are already reported in the literature. The piezoelectric materials considered in the present study are zinc oxide (ZnO) [33], lead zirconate titanate (Pb $[Zr_xTi_{1-x}]$ O_3) [34], $K_{0.5}Na_{0.5}NbO_3$-$LiSbO_3$ (KNN-LS) [35], KNN-LS doped with 1 wt.% $CaTiO_3$ (KNN-LS-CT (1 wt.%)) [35], KNN-LS doped with 2 wt.% $CaTiO_3$ (KNN-LS-CT (2 wt.%)) [35] and $0.885(Bi_{0.5}Na_{0.5})$ TiO_3-0.05 $(Bi_{0.5}K_{0.5})$ TiO_3-$0.015(Bi_{0.5}Li_{0.5})$ TiO_3-$0.05BaTiO_3$ (BNKLBT) [36]. PZT is one of the most commonly used piezoelectric materials for sensor application, energy harvesting and transducers due to its superior electromechanical coupling factor. BNKLBT is a lead-free piezoelectric material and has been used by authors in ultrasonic wirebonding transducers [36]. KNN-LS doped with 1 wt.% $CaTiO_3$ (KNN-LS-CT (1 wt.%)) and KNN-LS doped with 2 wt.% $CaTiO_3$ (KNN-LS-CT (2 wt.%)) are reported for enhanced electrical properties than the base composition of KNN-LS. Moreover, physical properties of KNN-LS-CT (1 wt.%) and KNN-LS-CT (2 wt.%) are temperature insensitive at a wide temperature range of −50 °C to 200 °C [35]. ZnO is another potential piezoelectric material [37]. Bowen et al. [38] provided a detailed review on piezoelectric energy harvesting associated with different piezoelectric materials. Piezoelectric materials and their physical properties are summarized in Table 1.

2.2. Methodology

Typical components of piezoelectric energy harvester are shown in Fig. 1, which consists of mechanical structure, piezoelectric material and electrical interference. The mechanical structure (mostly beam) is used as input source of mechanical energy (due to vibrations in structure). The piezoelectric material layer is bounded on the surface of the beam structure, which helps to convert mechanical energy into electrical energy (in the form of charge). The third component collects the charge and coverts it into usable electrical energy [39].

The present piezoelectric energy harvester is designed to take the advantage of d_{31} bending mode of piezoelectric materials which allows piezoelectric layers to be easily attached to the host layer [9,19,21,40–45]. Typically, unimorph cantilever piezoelectric energy harvester has one layer of the piezoelectric material adhered to the thin metallic host structure. To increase the average strain and stress level along the beam length, proof mass is attached at the tip of the cantilever. Proof mass also helps to adjust the natural frequency to a desired frequency range [9,45–47], thereby resulting in reduced dimension of the harvester and a compact design of piezoelectric energy harvester for the same natural frequency. Electrodes are connected to the external resistance or load, which affects the natural frequency of the harvester due to backward coupling of piezoelectric material in mechanical domain [48].

3. Finite element formulation

A coupled piezoelectric energy harvester based on finite element formulation to discretize the electromechanical coupling phenomenon between mechanical and electrical domains is being presented here. First-order shear deformation theory is used to account for the shear effect of the structure in thickness direction. To simplify the computation, linear piezoelectric theory has been assumed. Host layer made of metal or composite materials is sandwiched by piezoelectric layers. Top and bottom electrodes of piezoelectric layers are connected to the external resistance as shown in Fig. 2. At element level in the finite element formulation, 24 mechanical (6 at each node $-U_x, U_y, U_z, \theta_x, \theta_y, \theta_z$) and 1 electrical ($\phi$) degree of freedom at the node are considered of degenerated shell element as depicted in Fig. 3. Electromechanical equations of linear piezoelectric material can be written as [49]

$$\{D\} = [e]^T\{S\} + [\alpha]\{E\} \quad (1)$$

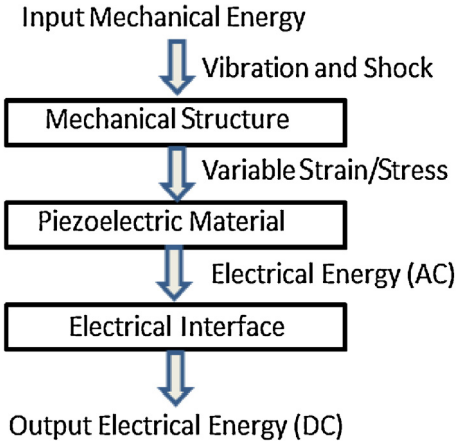

Fig. 1. Flow chart for piezoelectric energy harvesting.

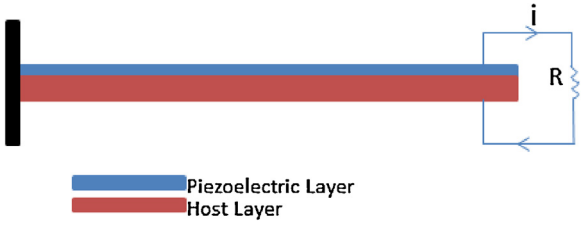

Fig. 2. Schematic for cantilever-type piezoelectric structure.

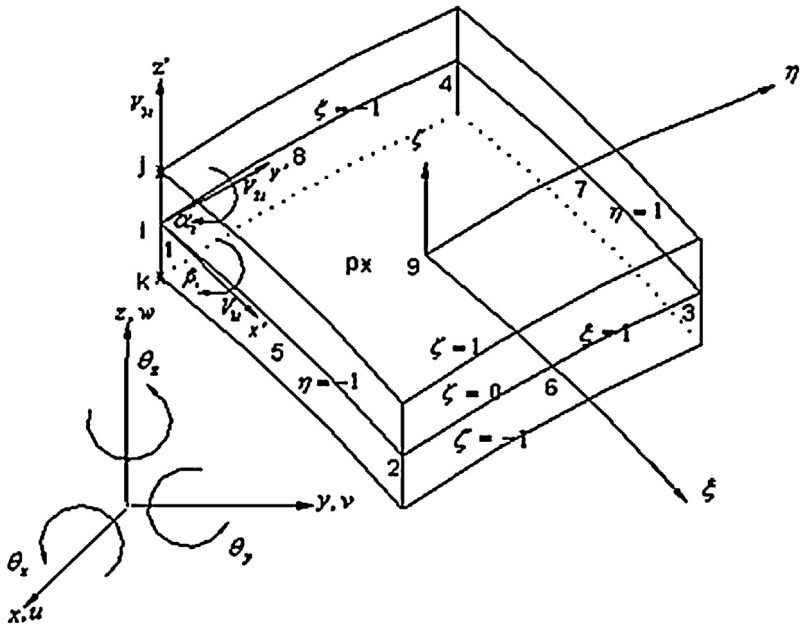

Fig. 3. Schematic of nine-noded degenerated shell element.

$$\{T\} = [\beta]\{S\} - [e]\{E\} \tag{2}$$

where $[D]$: electrical displacement, $[e]$: dielectric permittivity matrix, $[S]$: the strain vector, $[\alpha]$: the dielectric matrix at constant mechanical strain, $[\beta]$: the matrix of elastic coefficient at constant electrical field strength, $[E]$: the electrical field vector, and $[T]$: the stress vectors.

The above piezoelectric constitutive equations are in material coordinates. These are required to be converted to global coordinates. This can be done through transformation.

$$\{D\}_k = [\bar{e}]_k^T\{\varepsilon\}_k + [\bar{\alpha}]_k\{E\}_k \tag{3}$$

$$\{T\}_k = [\bar{\beta}]_k\{\varepsilon\}_k - [\bar{e}]_k\{E\}_k \tag{4}$$

where

$$[\bar{e}]_k = [T_v]^T[e]_k[T_o]_k[T_\varepsilon]$$

$$[\bar{\alpha}]_k = [T_v]^T[\alpha]_k[T_v]$$

$$[\bar{\beta}] = [T_\varepsilon]^T[T_o]_k^T[\beta]_k[T_o]_k[T_\varepsilon]$$

$[T_v]$, $[T_o]$ and $[T_\varepsilon]$ are vector transform matrix, orientation transformation matrix and strain transformation matrix, respectively. Detailed transformation matrices can be found in [50].

Using Hamilton's principle, the governing equation for the element can be written as

$$[M_{uu}]_e\{\ddot{r}\}_e + [C_{uu}]_e\{\dot{r}\}_e + [K_{uu}]_e\{r\}_e - [K_{\phi u}]_e\{v\}_e = \{F_m\}_e \tag{5}$$

$$[K_{\phi u}]_e\{r\}_e + [K_{\phi\phi}]_e\{v\}_e = \{Q\}_e \tag{6}$$

where $[M_{uu}]_e$ is the elemental mass matrix, $[K_{uu}]_e$ is the elemental stiffness matrix, $[K_{\phi u}]_e$ is elastic-electric coupling matrix for piezoelectric layer, $[K_{\phi\phi}]_e$ is the elemental electrical stiffness matrix, $[F_m]_e$ is applied mechanical force, $[Q]_e$ is the generated electrical charge due to backward coupling in electrical domain for an element, $[C_{uu}]_e$ is the damping matrix, $\{v\}_e$ is voltage across the layer and r is vibration resonance due to external force.

From the circuit theory, current flow through the resistance due to the charge Q is given as

$$i = -\frac{dQ}{dt} \tag{7}$$

Current across the resistance in terms of voltage is given as

$$i = \frac{v}{R} \tag{8}$$

From Eq. (6)

$$\frac{d}{dt}([K_{\phi u}]_e\{r\}_e + [K_{\phi\phi}]_e\{v\}_e) = \frac{d}{dt}\{Q\}_e$$

$$[K_{\phi u}]_e\{\dot{r}\}_e + [K_{\phi\phi}]_e\{\dot{v}\}_e = -\frac{\{v\}_e}{R} \tag{9}$$

$$[K_{\phi u}]_e\{\dot{r}\}_e + [K_{\phi\phi}]_e\{\dot{v}\}_e + \frac{\{v\}_e}{R} = 0$$

4. Optimization

Genetic algorithm is a broadly applicable random search technique based on the principles of natural selection and genetics. The GA starts with a randomly generated population. At the start of each iteration, a new population is generated. For the generation of a new population, the following steps are performed:

- Selection: In this step, two parent individuals are selected from the population on the basis of their fitness value.
- Crossover: The parents with better fitness value are allowed to take part in this step and to produce children using crossover arithmetic.
- Mutation: In this step, some chromosomes of the children are changed randomly according to mutation probability.
- The new offsprings are placed in the new population. This procedure is continued until termination criterion is met [51,52].

In this article, genetic algorithm (GA) is used to optimize the power density of piezoelectric energy harvester (PEH). GA is initiated with the population of random numbers or strings based on decision variables. Value of fitness function is evaluated based on random numbers. The fitness function in the present study is to maximize power density within selected frequency range. The decision variables considered to obtain optimized power density of piezoelectric energy harvester using different piezoelectric materials under study are load resistance (R), thickness of host layer (t_h)

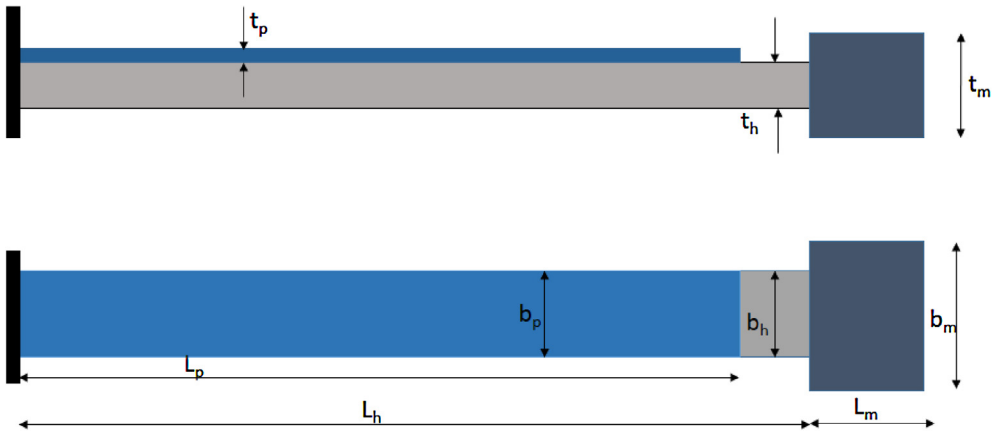

Fig. 4. Geometry of piezoelectric energy harvester.

and length of proof mass (L_m) (shown in Fig. 4). The schematic of the cantilever-type energy harvester consists of a top layer made of piezoelectric material that adheres to the host structure (shown in Fig. 4). A proof mass is attached to the tip of the cantilever to get the desired frequency range (resonant frequency). A little deviance from the resonant frequency causes huge reduction in power output of such harvesters. Hence, it is desired to optimize the parameters of the piezoelectric energy harvester to get maximum power output and power density.

Power of the harvester may be defined as [53]

$$P = \frac{v^2}{R} \tag{10}$$

where v is voltage across the resistance R.

Power density (η) for energy harvester is defined as the ratio of power (P) to harvester volume ($V = b_h L_h t_h + b_m L_m t_m + b_p l_p t_p$). Mean power density ψ over the specified frequency range $[f_1, f_2]$ is defined as

$$\psi = \int_{f_1}^{f_2} \frac{\eta}{(f_2 - f_1)} df = \int_{f_1}^{f_2} \frac{P}{(f_2 - f_1)(b_h L_h t_h + b_m L_m t_m + b_p l_p t_p)} df \tag{11}$$

where b, L, and t represent width, length and thickness, respectively. The subscripts h, m, and p represent the geometry of the host layer, proof mass and piezoelectric layer, respectively. The parameters used in numerical simulations for optimization process using GA are listed in Table 2.

In summary, the objective function of GA is to maximize the mean power (ψ) in the selected frequency range.

$$\text{Objective function :} \quad \max(\psi(\propto)) \quad \text{where} \quad \propto = f(R, L_m, t_h)$$

$$\text{Subject to :} \quad 10 \le L_m \le 40 \quad [\text{mm}]$$

$$0.75 \le t_h \le 2.00 \quad [\text{mm}]$$

$$1 \le R \le 100 \quad [\text{k}\Omega]$$

Table 2
Genetic algorithm parameters.

Simulation parameters for genetic algorithm	Value
Number of population size	30
Maximum generation	150
Number of bits by genes	8
Crossover probability	0.80
Mutation probability	0.10

5. Results and discussion

The geometric properties of host structure, piezoelectric material and proof mass are listed in Table 3. Table 1 presents the physical properties (mechanical and electrical) of different piezoelectric materials under study. The host structure is made up of brass (Young modulus: 103.4 GPa and density: 8410 kg/m^3). Base of the cantilever piezoelectric energy harvester is driven by harmonic force of amplitude 1 N, which acts as an input mechanical energy source for the harvester device. Performance of the energy harvester is investigated in the lower ambient frequency range 90–110 Hz as the environmental frequency is relatively low (normally less than 200 Hz) and random [54]. In the numerical simulations, damping ratio of 2% (structural damping) is assumed. The piezoelectric energy harvester is optimized for different piezoelectric materials using the Genetic Algorithm (GA) approach. The main aim of the present study was to optimize the PEH over a range of 90 Hz to 110 Hz to obtain maximum power density. For the same, Table 4 shows optimum value of resistance (R), length of proof mass (L_m) and thickness of host structure (t_h) obtained using GA for different piezoelectric materials under study. Thereafter, numerical simulations are carried out to calculate mean power and mean power density for different piezoelectric materials under study. The optimal parameters of PEH tabulated in Table 4 are used to calculate mean power and mean power density. Fig. 5 depicts the harvested power density for different piezoelectric materials under study over a frequency range of 90 Hz to 110 Hz. The mean power density of present PEH is also presented in Table 5. It is to be noted that the amplitude of power density and the mean power density is higher in case of KNN-LS-CT (2 wt.%) and KNN-LS-CT (1 wt.%) (Table 5). It is clear that the area under the curve for KNN-LS-CT (2 wt.%) and KNN-LS-CT (1 wt.%) is more than the area under the curve for ZnO, which indicated that the average value of power density is higher in excited frequency range (i.e. 90 Hz to 110 Hz) for former materials. Fig. 6 shows the harvested power of PEH

Table 3
Geometrical dimensions of host structure, piezoelectric material and proof mass.

Harvester properties	Value (mm)
Length of the host structure (L_h)	51
Length of piezoelectric ceramic (L_p)	50
Width of the host structure (b_h)	25
Width of piezoelectric ceramic (b_p)	25
Width of the proof mass (b_m)	40
Thickness of piezoelectric ceramic (t_p)	0.27
Thickness of the proof mass (t_m)	5

Table 4
Optimum values of the parameters using genetic algorithm.

Optimum variables	Piezoelectric materials					
	PZT	BNKLBT	KNNLS	KNN-LS-CT (1% wt)	KNN-LS-CT (2%wt)	ZnO
Resistance (kΩ)	2.15×10^4	8.75×10^4	2.42×10^4	5.26×10^4	8.71×10^4	9.96×10^4
Thickness (m)	1.09×10^{-3}	1.01×10^{-3}	1.27×10^{-3}	1.28×10^{-3}	1.57×10^{-3}	1.79×10^{-3}
Length (m)	1.16×10^{-2}	1.18×10^{-2}	1.71×10^{-2}	1.92×10^{-2}	2.70×10^{-2}	1.52×10^{-2}

Table 5
Harvested power and power density for different piezoelectric materials.

	Piezoelectric materials					
	PZT	BNKLBT	KNNLS	KNN-LS-CT (1% wt)	KNN-LS-CT (2%wt)	ZnO
Mean power (W)	9.71×10^{-3}	3.22×10^{-3}	1.32×10^{-2}	1.97×10^{-2}	2.68×10^{-2}	3.29×10^{-5}
Mean power density (W/cm^3)	2.19×10^{-3}	7.44×10^{-4}	2.30×10^{-3}	3.19×10^{-3}	3.31×10^{-3}	6.71×10^{-6}
Volume (cm^3)	4.41×10^{-6}	4.33×10^{-6}	5.75×10^{-6}	6.19×10^{-6}	8.10×10^{-6}	4.89×10^{-6}

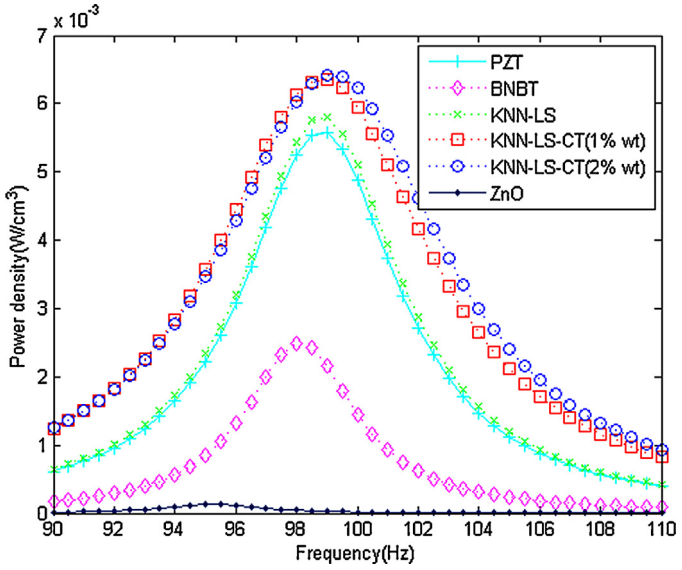

Fig. 5. Variation of harvested power density with frequency for different piezoelectric materials under investigation.

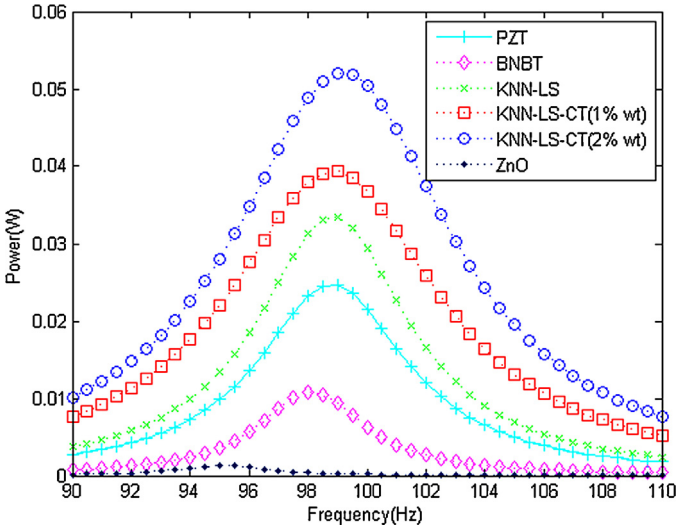

Fig. 6. Variation of harvested power with excited frequency for different piezoelectric materials under study.

within exciting frequency range for materials under investigation. The mean power of PEH within exciting frequency range is also presented in Table 5. It can be observed from the numerical simulation results that the PEH with a layer of KNN-LS-CT (2 wt.%) piezoelectric material is having maximum mean power than that of other piezoelectric materials considered in the present study. For the optimized design, mean power density for KNN-LS-CT (2 wt.%) is 3.6%, 30%, 97%, 35% and 77% higher than that of KNN-LS-CT (1 wt.%), KNN-LS, ZnO, PZT and BNKLBT materials, respectively. It indicates that the lead-free piezoelectric materials of the KNN-LS family are potential candidates to replace lead-based PZT for energy harvesting applications.

6. Conclusions

The performance of few important piezoelectric materials is simulated for unimorph-type cantilever piezoelectric energy harvester. The finite element method (FEM) is used to model the piezolaminated unimorph cantilever structure. The first-order shear deformation theory (FSDT) and linear piezoelectric theory are implemented in finite element simulations. The genetic algorithm (GA) optimization approach is carried out to optimize the structural parameters of mechanical energy-based energy harvester for maximum power density and power output. Results obtained from the finite element model show that the piezoelectric materials of KNN-LS-CT (2 wt.%) yield 35% higher mean power density than PZT material. This study shows that the KNN-LS family has enormous possibilities for piezoelectric energy harvester. Such study will be helpful to select the best piezoelectric material for cantilever-type energy harvester.

Acknowledgements

Rahul Vaish gratefully acknowledges financial support from Department of Science and Technology (DST), New Delhi, and Indian National Science Academy (INSA), India, under INSPIRE Faculty Award (ENG-01)-2011.

References

[1] R. Tashiro, N. Kabei, K. Katayama, Y. Ishizuka, F. Tsuboi and K. Tsuchiya, JSME Int. J.: Ser. C, 43, 916–922 (2000).
[2] P.D. Mitcheson, P. Miao, B.H. Stark, E. Yeatman, A. Holmes and T. Green, Sens. Actuators A, 115, 523–529 (2004).
[3] S. Meninger, J.O. Mur-Miranda, R. Amirtharajah, A. Chandrakasan and J.H. Lang, IEEE Trans. VLSI Syst., 9, 64–76 (2001).
[4] C. Williams and R.B. Yates, Sens. Actuators A, 52, 8–11 (1996).
[5] P. Glynne-Jones, M. Tudor, S. Beeby and N. White, Sens. Actuators A, 110, 344–349 (2004).

[6] D.P. Arnold, IEEE Trans. Magn., 43, 3940–3951 (2007).
[7] R. Amirtharajah and A.P. Chandrakasan, IEEE J. Solid-State Circ., 33, 687–695 (1998).
[8] S.P. Beeby, M.J. Tudor and N. White, Meas. Sci. Technol., 17, R175 (2006).
[9] Y. Jeon, R. Sood, J.-H. Jeong and S.-G. Kim, Sens. Actuators A, 122, 16–22 (2005).
[10] S. Roundy, P.K. Wright and J. Rabaey, Comput. Commun., 26, 1131–1144 (2003).
[11] S. Priya, J. Electroceram., 19, 167–184 (2007).
[12] G. Park, T. Rosing, M.D. Todd, C.R. Farrar and W. Hodgkiss, J. Infrastruct. Syst., 14, (6) 4–79 (2008).
[13] J.F. Tressler, S. Alkoy and R.E. Newnham, J. Electroceram., 2, 257–272 (1998).
[14] J.J. Dosch, D.J. Inman and E. Garcia, J. Intell. Mater. Syst. Struct., 3, 166–185 (1992).
[15] E.F. Crawley and J. De Luis, AIAA J., 25, 1373–1385 (1987).
[16] W.W. Clark, J. Intell. Mater. Syst. Struct., 11, 263–271 (2000).
[17] K. Cook-Chennault, N. Thambi and A. Sastry, Smart Mater. Struct., 17, 043001 (2008).
[18] D. Koyama and K. Nakamura, Ultrason. Symp. (IUS): IEEE, 1973–1976 (2009).
[19] H.A. Sodano, G. Park and D. Inman, Strain, 40, 49–58 (2004).
[20] K. Swee-Leong, N. Mohamad, Y. Weng, C.S. Kien and D.C. Fu, INECCE-IEEE, 420–423 (2011).
[21] S. Roundy and P.K. Wright, Smart Mater. Struct., 13, 1131 (2004).
[22] H.A. Sodano, D.J. Inman and G. Park, Shock Vib. Digest, 36, 197–206 (2004).
[23] T. Ng and W.J. Liao, Intell. Mater. Syst. Struct., 16, 785–797 (2005).
[24] T. Takenaka and H. Nagata, J. Eur. Ceram. Soc., 25, 2693–2700 (2005).
[25] M.D. Maeder, D. Damjanovic and N. Setter, J. Electroceram., 13, 385–392 (2004).
[26] Y. Saito, H. Takao, T. Tani, T. Nonoyama, K. Takatori, T. Homma, T. Nagaya and M. Nakamura, Nature, 432, 84–87 (2004).
[27] S. Zhang, R. Xia and T.R. Shrout, J. Electroceram., 19, 251–257 (2007).
[28] T.R. Shrout and S.J. Zhang, J. Electroceram., 19, 113–126 (2007).
[29] P. Panda, J. Mater. Sci., 44, 5049–5062 (2009).
[30] A. Chauhan and R. Vaish, Adv. Sci. Eng. Med., 5, 715–719 (2013).
[31] R. Vaish, Int. J. Appl. Ceram. Technol., (2012).
[32] G. Vats and R. Vaish, J. Adv. Ceram., 2, 141–148 (2013).
[33] J. Ding, V.R. Challa, M. Prasad and F.T. Fisher, Selected Topics in Micro/Nano-robotics for Biomedical Applications, Springer (2013).
[34] M. Zhu, E. Worthington and A. Tiwari, Ultrason: IEEE. Trans Ultrason. Ferrelectr., 57, 427–437 (2010).
[35] S. Zhang, R. Xia and T.R. Shrout, Appl. Phys. Lett., 91, (2007).
[36] H. Chan, S. Choy, C. Chong, H. Li and P. Liu, Ceram. Int., 34, 773–777 (2008).
[37] J. Briscoe, M. Stewart, M. Vopson, M. Cain, P.M. Weaver and S. Dunn, Adv. Energy Mater., 2, 1261–1268 (2012).
[38] C. Bowen, H. Kim, P. Weaver and S. Dunn, Energy Environ. Sci., 7, 25–44 (2014).
[39] E. Lefeuvre, M. Lallart, C. Richard and D. Guyomar, Piezoelectric Ceramics, InTech Europe (2010), pp. 165–184.
[40] H. Xue, Y. Hu and Q.-M. Wang, Ultrason. IEEE: Trans Ultrason. Ferrelectr., 55, 2104–2108 (2008).
[41] J. Dietl, A. Wickenheiser and E. Garcia, Smart Mater. Struct., 19, 055018 (2010).
[42] M. Arafa, O. Aldraihem and A. Baz, J. Vib. Acoust., 134, 031004 (2012).
[43] N.E. DuToit and B.L. Wardle, AIAA J., 45, (112) 6–1137 (2007).
[44] A. Erturk and D. Inman, Smart Mater. Struct., 18, 025009 (2009).
[45] M. Kim, M. Hoegen, J. Dugundji and B.L. Wardle, Smart Mater. Struct., 19, 045023 (2010).
[46] D. Shen, J.-H. Park, J. Ajitsaria, S.-Y. Choe, H.C. Wikle III and D.-J. Kim, J. Micromech. Microeng., 18, 055017 (2008).
[47] H.-B. Fang, J.-Q. Liu, Z.-Y. Xu, L. Dong, L. Wang, D. Chen, B.-C. Cai and Y. Liu, Microelectron. J., 37, 1280–1284 (2006).
[48] F. Lu, H. Lee and S. Lim, Smart Mater. Struct., 13, 57 (2004).
[49] A. Erturk and D.J. Inman, Piezoelectric Energy Harvesting, Wiley.Com (2011).
[50] R. Kumar, B. Mishra and S. Jain, Finite Elem. Anal. Des., 45, 13–24 (2008).
[51] D.E. Goldberg and J.H. Holland, Mach. Learn., 3, (9) 5–99 (1988).
[52] D. Kalyanmoy, Optimization for Engineering Design: Algorithms and Examples, PHI Learning Pvt. Ltd. (2004).
[53] Y. Shu and I. Lien, Smart Mater. Struct., 15, (1499) (2006).
[54] S.J. Roundy, Energy Scavenging for Wireless Sensor Nodes with a Focus on Vibration to Electricity Conversion, University of California (2003).